ACS APPLIED MATERIALS & INTERFACES

Research Article

Cite This: ACS Appl. Mater. Interfaces 2017, 9, 38530-38536

www.acsami.org

Interfacial Engineering with Cross-Linkable Fullerene Derivatives for High-Performance Perovskite Solar Cells

Tin Kang, Cheng-Min Tsai, Yu-He Jiang, Ganesh Gollavelli, Nayantara Mohanta, Eric Wei-Guang Diau,* and Chain-Shu Hsu*

Department of Applied Chemistry and Institute of Molecular Science, National Chiao Tung University, 1001 Ta Hsueh Road, Hsinchu 30010, Taiwan

Supporting Information

ABSTRACT: Two fullerene derivatives with styryl and oxetane cross-linking groups served as interfacial materials to modify an electron-transporting layer (ETL) of TiO_2, doped with Au nanoparticles, processed under low-temperature conditions to improve the performance of perovskite solar cells (PSC). The cross-linkable [6,6]-phenyl-C_{61}-butyric styryl dendron ester was produced via thermal treatment at 160 °C for 20 min, whereas the cross-linkable [6,6]-phenyl-C_{61}-butyric oxetane dendron ester (C-PCBOD) was obtained via UV-curing treatment for 45 s. Both cross-linked fullerenes can passivate surface-trap states of TiO_2 and have also excellent surface coverage on the TiO_2 layer shown in the corresponding atomic force microscopy images. To improve the crystallinity of perovskite, we propose a simple co-solvent method involving mixing dimethylformamide (DMF) and dimethyl sulfoxide (DMSO) in a specific ratio (DMF/DMSO = 90/10). The fullerene derivative layer between the ETL and perovskite layers significantly improved electron extraction and suppressed charge recombination by decreasing the density of traps at the ETL surface. A planar PSC device was fabricated with the configuration indium tin oxide/TiO_2 (Au)/C-PCBOD/perovskite/spiro-OMeTAD/Au to attain a power conversion efficiency (PCE) of 15.9%. The device performance was optimized with C-PCBOD as an interfacial mediate to modify the surface of the mesoporous TiO_2 ETL; the C-PCBOD-treated device attained a significantly enhanced performance, PCE 18.3%. Electrochemical impedance spectral and photoluminescence decay measurements were carried out to understand the characteristics of electron transfer and charge recombination of the perovskite/TiO_2 samples with and without a fullerene interfacial layer.

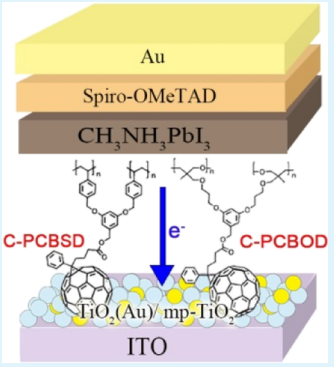

KEYWORDS: *cross-linkable fullerene, ETL, electrochemical impedance spectroscopy, interfacial layer, photoluminescence decay, PSC, titanium oxide*

INTRODUCTION

Perovskite solar cells (PSCs) have attracted much attention because of the rapid progress of their device performance, which has become comparable with that of Si-based solar cells.[1−5] A traditional mesoscopic PSC contains a mesoporous TiO_2 (mp-TiO_2) layer to serve as an electron-transporting layer (ETL) and with 2,2′,7,7′-tetrakis(*N*,*N*-di-*p*-methoxyphenylamine)-9,9-spirobifluorene (spiro-OMeTAD) to serve as a hole-transporting layer (HTL).[6] Alternatively, planar heterojunction (PHJ) PSCs have been reported to have either a normal n−i−p or an inverted p−i−n configuration with ETLs and HTLs of varied types.[7] For a normal PHJ PSC, with an n−i−p structure, the most popular ETL materials are ZnO and TiO_2.[8,9] Although ZnO can be prepared by a low-temperature sol−gel process and large electron mobility, a ZnO-based PSC suffers from thermal instability, such that perovskite crystals are readily decomposed into PbI_2.[10] Using TiO_2 as the ETL to fabricate high-performance PSCs has hence been widely applied because the TiO_2/perovskite interlayer is thermally more stable. Most high-performance PHJ PSCs were prepared with a compact TiO_2 layer prepared by high-temperature sintering, which prevents it from being used in a roll-to-roll process to fabricate flexible PSC devices.

Strategies of low-temperature processing of TiO_2 to serve as an ETL for PSCs have also been reported,[11−13] but the electron mobility of a low-temperature TiO_2 layer is small, about 0.1−4 $cm^2\ V\ s^{-1}$ for a single crystal,[8,14] and the surfaces of these TiO_2 layers might contain abundant electron traps that disturb the electron transport and result in severe hysteresis of the device. Fullerene derivatives have been reported to modify the TiO_2 surface by decreasing the density of interfacial defect sites of TiO_2.[15] For this purpose, Snaith and Jen and their co-workers proposed a fullerene-based self-assembling monolayer (SAM) to anchor the fullerene derivatives on the TiO_2 surface,[16,17] but this C_{60} SAM-based approach suffers from an incomplete coverage of the TiO_2 surface and requires an extended duration to process. Wojciechowski et al.[18] proposed cross-linkable fullerene derivatives of two types to modify only the fluorine-doped tin oxide (FTO) electrode; one type uses sol−gel C_{60}

Received: August 8, 2017
Accepted: October 18, 2017
Published: October 18, 2017

DOI: 10.1021/acsami.7b11795
ACS Appl. Mater. Interfaces 2017, 9, 38530−38536

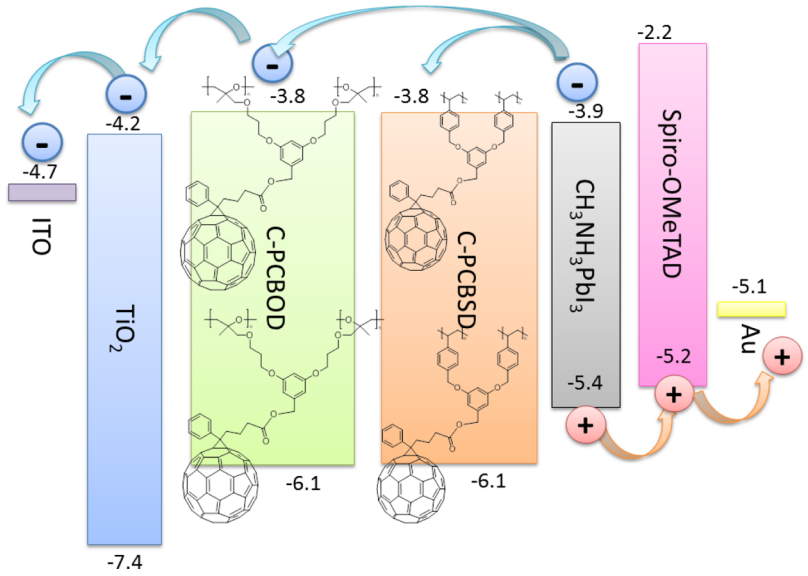

Figure 1. Schematic diagram of an n−i−p planar heterojunction PSC with potential−energy levels of each layer. Either C-PCBOD or C-PCBSD cross-linked fullerene served as an interfacial layer between TiO_2 and perovskite.

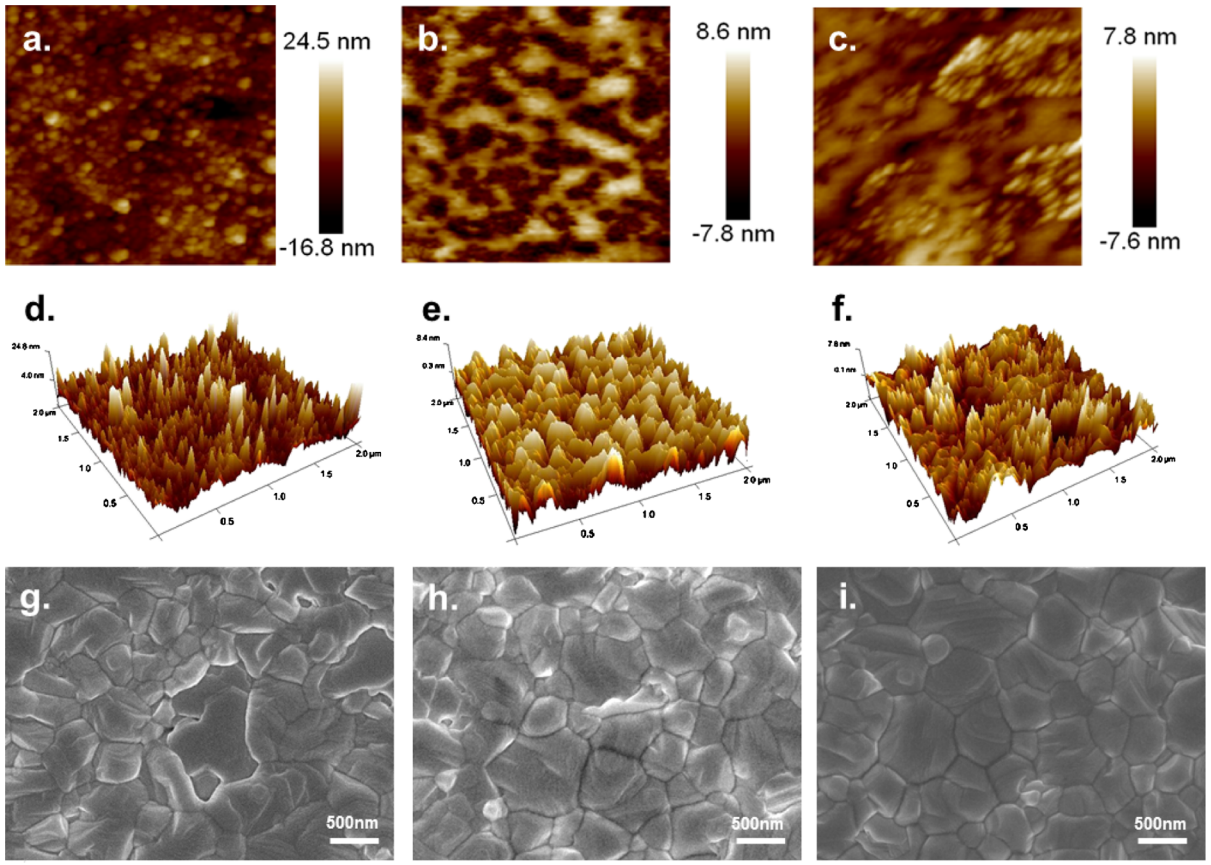

Figure 2. Images from an atomic force microscope (AFM) showing the surface morphology for (a,d) TiO_2 (Au), (b,e) C-PCBSD, and (c,f) C-PCBOD. Top-view images from a scanning electron microscope (SEM) of perovskite layers are shown for perovskite deposited on (g) TiO_2 (Au), (h) C-PCBSD, and (i) C-PCBOD.

cross-linked on exposure to trifluoroacetic acid vapor, whereas the second type involves a thermally cross-linkable fullerene phenyl-C61-butyric acid benzocyclobutene ester (PCBCB) to form an insoluble interfacial layer. For the sol−gel C_{60} using the vapor-cross-linked process, however, one must use an acidic vapor, which might form a residue on the surface; the acid is likely to affect the crystallization of the perovskite layer. The second approach involves raising the temperature to 200 °C to form cross-linked PCBCB, which might prevent its application for flexible photovoltaic devices.

In this work, we utilized [6,6]-phenyl-C_{61}-butyric styryl dendron ester (PCBSD) and [6,6]-phenyl-C_{61}-butyric oxetane

DOI: 10.1021/acsami.7b11795
ACS Appl. Mater. Interfaces 2017, 9, 38530−38536

dendron ester (PCBOD) as cross-linkable agents to modify the surface of TiO_2 for PSC application. The results demonstrate that PCBSD can be thermally cross-linked in 20 min at 160 °C, whereas PCBOD can be UV-curable in 45 s; both cross-linked fullerenes (represented as C-PCBSD and C-PCBOD, respectively) have superior surface coverage for the TiO_2 layer. Furthermore, the cross-linked C-PCBSD or C-PCBOD interfacial layer has a solvent-resistant characteristic that prevents it from being washed away in the subsequent spin-casting of the perovskite layer. Moreover, both C-PCBSD and C-PCBOD interlayers can passivate surface trap states of the TiO_2 layer. We incorporated Au nanoparticles (NPs) into the TiO_2 layer to enhance its electron mobility. Both photoluminescence (PL) decay and electrochemical impedance spectral (EIS) measurements were undertaken to understand the characteristics of electron transfer and charge recombination of the perovskite/TiO_2 samples with and without a fullerene interfacial layer. The normal PHJ PSC devices with C-PCBSD and C-PCBOD interfacial layers eventually attained power conversion efficiency (PCE) of 15.3 and 15.9%, respectively, which are much greater than for a reference cell without a fullerene interfacial layer. The cross-linked C-PCBOD was also used to modify the mp-TiO_2 surface for a mesoscopic PSC to attain the PCE of 18.3%, with a fill factor (FF) significantly improved relative to a reference cell without the C-PCBOD treatment.

RESULTS AND DISCUSSION

Figure 1 depicts the device structures of a PSC with or without ETL-modified layers. TiO_2 NPs were mixed with Au NPs in ethanol and spin-cast onto indium tin oxide (ITO) glass substrates. A solution of PCBSD or PCBOD was spin-coated onto TiO_2 (Au) ETL and then cross-linked with a thermal treatment or UV radiation. The perovskite layer was deposited using a modified two-step method; a chlorobenzene solution of spiro-OMeTAD was spin-coated on top of the perovskite layers to serve as the HTL. A gold electrode was finally deposited on top of the spiro-OMeTAD layer by thermal evaporation.

Figure 2a–f shows images of bare TiO_2 (Au), C-PCBSD, and C-PCBOD surfaces from an AFM. The C-PCBOD showed a surface much smoother than that of bare TiO_2 (Au) and C-PCBSD; the AFM root-mean-square (rms) roughness of the C-PCBOD surface was 1.38 nm; and the rms roughnesses of C-PCBSD and bare TiO_2 (Au) surfaces were 2.73 and 5.41 nm, respectively. Figure 2g–i shows SEM images of three perovskite layers prepared on top of bare TiO_2 (Au), C-PCBSD, and C-PCBOD at the same rate of spin-coating and the same concentration of PbI_2. The grain size of the perovskite on both C-PCBSD and C-PCBOD surfaces distributed evenly with the largest grain size up to about 1 μm, whereas the grain size of the perovskite on bare TiO_2 (Au) revealed an uneven distribution. The smooth underlayer is favorable for the crystallization of a perovskite active layer.[19] As shown in our AFM images, the cross-linked fullerene interfacial layers have surfaces smoother than the bare TiO_2 (Au) layer, which might be the reason for perovskite to form crystals larger and more uniform for the former than for the latter.

The π-electrons of the fullerene derivatives have a positive electron affinity for transporting electrons.[20,21] Both C-PCBSD and C-PCBOD interfacial layers can thus facilitate electron transport for their devices. Even though PbI_2/*N*,*N*-dimethyl formamide (DMF) and dimethyl sulfoxide (DMSO) were reported to be harmful to the [6,6]-phenyl-C_{61}-butyric acid methyl ester (PCBM) layer because of the solubility of PCBM in those solvents that are used to dissolve perovskite precursors,[22,23] the cross-linked fullerene derivatives that we propose herein have the ability to prevent the cross-linked fullerene interfacial layers from being washed out by those solvents, as reported elsewhere.[24,25]

A conventional two-step method to prepare perovskite has disadvantages of an uncontrollable size of perovskite crystals and the presence of residual PbI_2 in the perovskite layer because of incomplete transformation in the second step.[20,26] In this work, we modified the traditional two-step method by adding DMSO in varied amounts into a DMF solution to facilitate the growth of perovskite crystals because DMSO has a high boiling point and small saturated vapor pressure. Furthermore, DMSO coordinates strongly with Pb^{2+} through its electronegative atoms (oxygen) to produce stable DMSO–PbI_2 complexes that can retard the crystallization of PbI_2.[20] Figure S1, Supporting Information, displays SEM images of perovskite prepared with mixed solvents using DMSO fractions varied from 0 to 90%. The perovskite layer obtained with DMSO (10%) shows a smooth morphology free of pin holes. When the fraction of DMSO increased to more than half, pin holes and an incomplete surface coverage occurred. These results might be due to excess stable DMSO–PbI_2 complexes, which cluster together and form large perovskite grains; the volatile DMF vaporizes quickly to form pin holes and voids. We hence chose a co-solvent with a ratio of 10/90 of DMSO/DMF as an optimized condition for the further fabrication of a perovskite active layer.

X-ray diffraction (XRD) was implemented to ensure that the conversion of PbI_2 into $CH_3NH_3PbI_3$ was complete. Figure S2, Supporting Information, shows XRD patterns of a PbI_2 sample and the perovskite active layers prepared by a conventional two-step method and our modified two-step co-solvent method. The (001) signal of PbI_2 is clearly observed for the perovskite prepared by a conventional two-step method but is completely absent from the perovskite fabricated with our modified co-solvent method.

To enhance the electron extraction of the TiO_2 ETL, we incorporated Au NPs into the TiO_2 ETL as proposed by Zhang et al. for a polymer solar cell.[27] According to their results, the Au NP can absorb light, generate hot carriers by plasmonic-electric effects, and fill the trap states of TiO_2 NPs; the electron mobility of the TiO_2 ETL became thereby enhanced. We synthesized the TiO_2 NP by a low-temperature nonaqueous method and with a particle size of ~13 nm. The TiO_2 nanocrystals were dispersed in ethanol and Au NPs were added in varied amounts. To derive the optimal Au NP concentration, we fabricated P3HT:$PC_{61}BM$ solar cells with Au NPs at varied concentrations in TiO_2. Table S1, Supporting Information, summarizes the *J*–*V* characteristics of polymer solar cells prepared with Au NPs at varied concentrations. These results demonstrate that the best PCE values were obtained for the TiO_2 layer prepared with an Au solution (10 and 30 vol %) with respect to the TiO_2 precursor solution. We used the space-charge-limited current (SCLC) method to investigate the enhanced carrier mobility for devices made with the configuration ITO/TiO_2 (Au)/C-PCBSD/P3HT:$PC_{61}BM$/Ca/Al (Figure S3, Supporting Information). The results are summarized in Table S2, Supporting Information; the device made with an Au NP concentration of 30 vol % showed the greatest carrier mobility, 4.54×10^{-4} cm^2 V^{-1} s^{-1}. We hence used the TiO_2 precursor solution containing Au NPs (30 vol

DOI: 10.1021/acsami.7b11795
ACS Appl. Mater. Interfaces 2017, 9, 38530–38536

%) to prepare the TiO_2 (Au) layer as the ETL for the present work.

Figure 3a,b shows the best $J-V$ curves and spectra of the efficiency of conversion of IPCE, respectively, for PSC devices

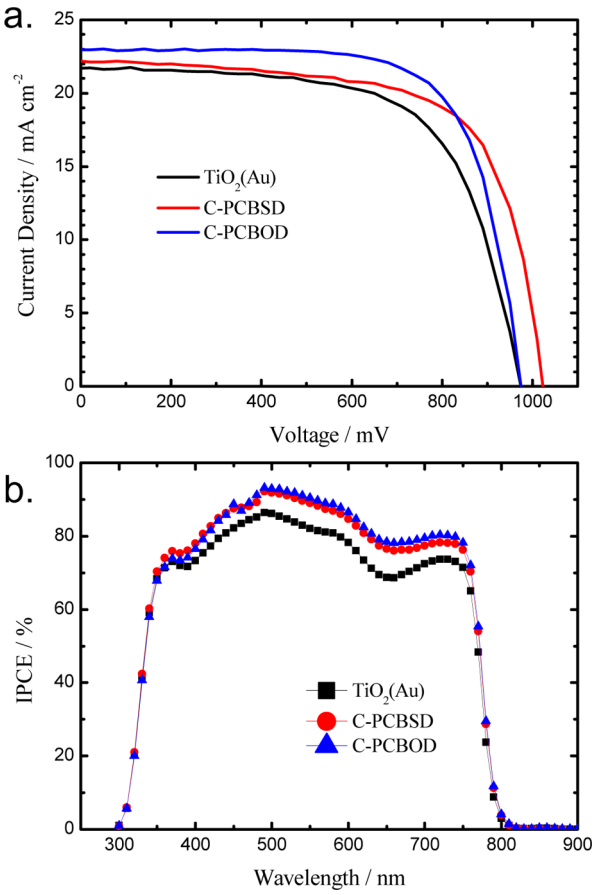

Figure 3. (a) $J-V$ characteristics and (b) efficiency of conversion of incident photons to power (IPCE) of PSC with and without interfacial layers of cross-linked fullerene.

fabricated with either a C-PCBSD or a C-PCBOD interfacial layer compared with a reference TiO_2 (Au) cell without interfacial layers of cross-linked fullerene; the average photovoltaic parameters are summarized in Table 1; the corresponding raw data of ten devices are listed in Tables S3–S5, Supporting Information. The reference PSC device shows a PCE of 13.0 ± 0.5%, poorer than that modified with C-PCBSD (PCE 14.7 ± 0.3%) and C-PCBOD (PCE 15.4 ± 0.4%); a device modified with a C-PCBOD interfacial layer showed the best performance, PCE 15.9%. To test the effect of hysteresis of the C-PCBOD device, we obtained $J-V$ curves for both reverse and forward directions at scan rates of 0.05, 0.15 and 0.3 V/s, shown in Figure S4a–c, Supporting Information, respectively. The results indicate that hysteresis was involved to a certain extent at a large scan rate but was small at a small scan rate. The stabilized power output of the C-PCBOD device measured at the point of maximum power is shown in Figure S5, Supporting Information, for which the maximum power sustained a constant PCE value for 10 min under 1 sun irradiation. We tested also the effect of varied C-PCBOD concentrations on device performance, which showed that a precursor condition with PCBOD (7 mg) dissolved in dichlorobenzene (DCB, 1 mL) gave the best PCE (Figure S6, Supporting Information).

For the IPCE results shown in Figure 3b, both C-PCBSD and C-PCBOD devices exhibited a substantial improvement in the spectral range of 400–750 nm compared with the reference cell. Integrating the IPCE of three devices over the AM 1.5G solar spectrum yielded calculated short-circuit photocurrent densities slightly less than, but within experimental uncertainties of, that obtained from a $J-V$ measurement (Table S6, Supporting Information). Such significant improvements in the IPCE values might be due to the increased thickness of the perovskite film after passivation of the TiO_2 (Au) surface with our cross-linked fullerene derivatives. According to the cross-sectional SEM images shown in Figure S7, Supporting Information, the thicknesses of the perovskite layers of the three devices are similar (230–250 nm). The enhanced IPCE values hence indicate that the interfacial layers of cross-linked fullerene play an important role for charge extraction so as to enhance J_{sc} of both C-PCBSD and C-PCBOD devices.

To characterize the internal resistance and charge-transfer kinetics of the PSC with various modifications, we measured EIS spectra under 1 sun illumination with a bias voltage at the V_{oc} value. Figure S8, Supporting Information, presents Nyquist plots covering the frequency range from 100 mHz to 4 MHz; the simulated EIS results according to the equivalent circuit model (Figure S9, Supporting Information) are summarized in Table S7, Supporting Information. The EIS results show Nyquist plots that feature two semicircles: the high-frequency impedance (R_{hf}) reflects charge transfer at the perovskite/ETL interface, whereas the low-frequency impedance (R_{lf}) reflects charge recombination at the same interface. Our results show that both C-PCBOD and C-PCBSD devices containing interfacial layers of cross-linkable fullerene have much decreased R_{hf} and increased R_{lf} values relative to the reference cell. These results imply that the electron transfer is more efficient and the charge recombination is less efficient in the presence of the C-PCBOD and C-PCBSD interfacial layers than with no interfacial layer for the reference cell. The decreased charge-transfer resistance of both C-PCBOD and C-PCBSD devices is due to the greater electron affinity of those cross-linked fullerene layers, which facilitates an efficient electron transfer from the perovskite to TiO_2 (Au) ETL.

Figure 4 shows time-resolved PL decay curves of perovskite samples deposited on TiO_2 with or without interfacial layers of cross-linked fullerene measured by the time-correlated single-photon counting (TCSPC) technique reported elsewhere.[28] Fitting the PL transients with a biexponential decay function yielded the corresponding lifetimes with relative amplitudes

Table 1. Average Photovoltaic Parameters of Ten Low-Temperature TiO_2 Planar PSC Devices (Metal Mask Area 0.04 cm^2) with or without Cross-Linkable Fullerene Interfacial Layers; the Largest PCE Values are Represented in Parentheses

device	J_{sc}/mA cm^{-2}	V_{oc}/V	FF/%	PCE/%
TiO_2 (Au)	20.70 ± 0.59	0.984 ± 0.023	63.9 ± 1.6	13.0 ± 0.5 (13.7)
C-PCBSD	21.94 ± 0.27	1.010 ± 0.022	66.4 ± 1.5	14.7 ± 0.3 (15.3)
C-PCBOD	22.22 ± 0.37	1.012 ± 0.019	68.5 ± 2.3	15.4 ± 0.4 (15.9)

DOI: 10.1021/acsami.7b11795
ACS Appl. Mater. Interfaces 2017, 9, 38530–38536

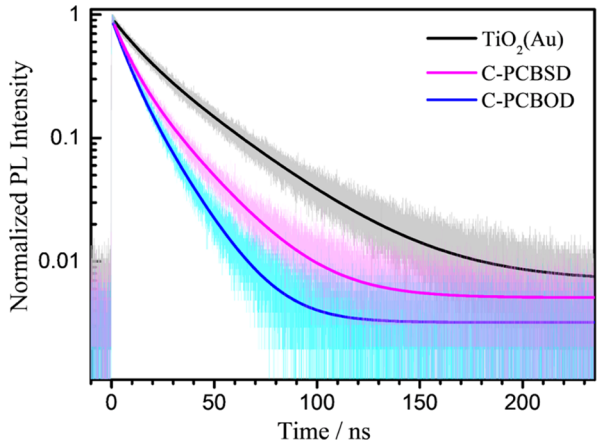

Figure 4. Time-resolved PL of perovskite deposited on TiO_2 (Au) with and without interfacial layers of cross-linked fullerene.

shown in Table 2. The first decay component (τ_1) in the PL decays is associated with electron injection at the perovskite/ETL interface, whereas the second decay component (τ_2) might be associated with the defect-state relaxation or electron transfer from bulk perovskite to the TiO_2 (Au) layer. The TCSPC results show that the lifetimes of perovskites would become much shorter with the layers of cross-linked fullerene than without those interfacial treatments in the reference cell, indicating that the electron transfer at the perovskite/ETL interface is more efficient for the C-PCBSD and C-PCBOD devices than for the reference cell. These TCSPC results are consistent with the EIS results that show superior charge extraction characteristic for both cross-linkable fullerene derivatives. C-PCBOD exhibits a charge extraction better than C-PCBSD, which is also reflected in the device performance shown in Figure 3.

Table 2. Lifetimes (Relative Amplitudes) of Perovskites Deposited on TiO_2 (Au) with and without Cross-Linked Fullerene Layers Measured by TCSPC, Excitation at 635 nm, Probe at 770 nm

sample	$\tau_1(A_1)$/ns	$\tau_2(A_2)$/ns	τ_{PL}[a]/ns
TiO_2 (Au)	11.80 ± 0.10 (0.36)	34.34 ± 0.11 (0.58)	30.37 ± 0.11
C-PCBSD	7.47 ± 0.04 (0.52)	22.20 ± 0.08 (0.42)	17.87 ± 0.06
C-PCBOD	6.77 ± 0.04 (0.50)	15.98 ± 0.08 (0.43)	12.94 ± 0.06

[a]The average lifetime was calculated with this statistical definition: $\tau_{PL} = \frac{\sum A_i \tau_i^2}{\sum A_i \tau_i}$, in which τ_i represents lifetimes and A_i represents the corresponding amplitudes of each component.

The above results are based on devices made with a planar heterojunction structure indicated in Figure 1. To enhance the surface contact between the TiO_2 and the interfacial layer, we optimized the photovoltaic performance of the C-PCBOD device based on a mesoporous TiO_2 (mp-TiO_2) layer of thickness ~200 nm.[29] The top-view SEM images of the mp-TiO_2 layer with and without C-PCBOD treatment shown in Figure S10, Supporting Information, disclose no discrepancy between both films because the C-PCBOD interfacial layer was too thin to be observable on that size scale. The mesoscopic cell has the device architecture FTO/mp-TiO_2/C-PCBOD/perovskite/spiro-OMeTAD/Ag, of which the perovskite active layer is made by a one-step adduct method.[30] Ten devices were fabricated under the same experimental conditions with and without the C-PCBOD interfacial layer; their corresponding photovoltaic parameters are listed in Tables S8 and S9, Supporting Information, respectively. Figure 5 shows optimized

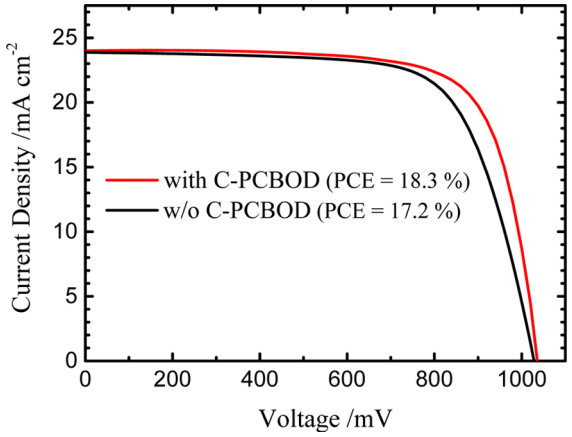

Figure 5. $J-V$ characteristics of PSCs based on mp-TiO_2 with and without interfacial layers of cross-linked fullerene C-PCBOD.

$J-V$ curves of the mp-TiO_2-based device with and without the C-PCBOD interfacial layer; the corresponding IPCE spectra are shown in Figure S11, Supporting Information. The C-PCBOD treatment improved the FF of the devices, relative to the planar device, from 67.6 ± 3.0% (without C-PCBOD) to 71.6 ± 2.4% (with C-PCBOD), which improved the PCE from the former at 16.5 ± 0.7% to the latter at 17.5 ± 0.6%, with the best device showing a PCE of 18.3%. We attribute such an improvement to the smaller contact resistance and greater electron affinity of the C-PCBOD interfacial layer, which facilitates electron transfer in the mp-TiO_2/perovskite interface for a device performance for the C-PCBOD cell, greater than that of a reference cell.

CONCLUSIONS

We used two cross-linked fullerene derivatives, C-PCBSD and C-PCBOD, as interfacial layers to enhance the performance of PSCs with TiO_2 (Au) prepared under low-temperature conditions as the ETL. Co-solvents DMF and DMSO facilitated the crystallization of perovskite to form uniform and closely packed crystals. The XRD results demonstrate that PbI_2 is completely converted to perovskite by this co-solvent method. The SEM images show a morphology of the perovskite layer free of pin holes at the best condition with the DMSO/DMF ratio of 10/90. EIS measurements demonstrate that devices with C-PCBSD and C-PCBOD layers show smaller charge-transfer impedance (R_{hf}) and larger charge-recombination impedance (R_{lf}) than for the reference cell. The transient PL decay profiles of the perovskite samples deposited with C-PCBSD and C-PCBOD show much shorter PL lifetimes than that without the interfacial layer, indicating that electron extraction is more efficient for the devices with the interfacial layers than for the reference cell. Photovoltaic measurements show that incorporation of C-PCBSD and C-PCBOD interfacial layers in the PHJ devices with an n−i−p configuration exhibits a substantially improved J_{sc} to enhance the device performance for the C-PCBSD and C-PCBOD devices, to attain the PCE of 15.3 and 15.9%, respectively, which is much greater than the reference cell (PCE of 13.7%). When this approach was applied to a mesoscopic device with

DOI: 10.1021/acsami.7b11795
ACS Appl. Mater. Interfaces 2017, 9, 38530−38536

C-PCBOD deposited on the mp-TiO_2 layer, the device performance was further improved to 18.3% with an enhanced FF compared with the reference cell. Our present results hence demonstrate that cross-linked fullerenes C-PCBSD and C-PCBOD serve as an excellent interfacial layer between the ETL and perovskite to enhance significantly the device performance because of their excellent electron-extraction characteristics and retarded charge recombination that was confirmed with both TCSPC and EIS measurements.

EXPERIMENTS

Materials. PbI_2, CH_3NH_3I, and spiro-OMeTAD (FrontMaterials Co. Ltd, Taiwan) and all other chemicals (purchased from Aldrich) were used as received. PCBSD and C-PCBOD were synthesized according to previous reports.[25,31] For the preparation of TiO_2 NP, $TiCl_4$ (1 mL) was introduced into a glass vial containing anhydrous ethanol (5 mL). Anhydrous benzyl alcohol (20 mL) was added; the container was left open with the entire mixture at 80 °C and continuously stirred for about 11 h. The white precipitate was washed several times with ethanol and then centrifuged to isolate the TiO_2 NPs. The TiO_2 NPs were dried in ambient air; a stock solution (10 mg mL^{-1} in ethanol) was prepared before use. The Au NP solutions were prepared according to a procedure reported elsewhere.[26]

Device Fabrication. ITO glass substrates (purchased from Wintek; sheet resistance 30 Ω sq^{-1}) were cleaned with detergent, deionized water, acetone, and isopropyl alcohol (IPA) in an ultrasonic bath for 15 min. The cleaned ITO glass substrates were dried overnight in an oven at >100 °C. The mixed TiO_2 NP/Au NP solution at a specific volume ratio (e.g., vol/vol = 100/30) was spin-coated on ITO at 6000 rpm for 80 s and annealed at 160 °C for 10 min to form the ETL. The cross-linkable PCBSD was dissolved in DCB at a concentration of 7 mg mL^{-1} and deposited onto the TiO_2 layer on spin-coating at 6000 rpm for 30 s. The substrate with the PCBSD layer was then transferred to a hotplate and annealed at 160 °C for 20 min to obtain a cross-linked PCBSD (C-PCBSD). For the C-PCBOD interlayer, a DCB solution containing PCBOD (7 mg mL^{-1}) and diphenyliodonium hexafluoroarsenate (6 mass % with respect to PCBOD) was spin-coated on the TiO_2 film at 6000 rpm for 30 s to form a thin film. The film as-cast was subsequently kept under UV treatment for 45 s in the glovebox for cross-linking.

For the perovskite crystals prepared by the two-step co-solvent method, the PbI_2 precursor solutions (460 mg mL^{-1}) were prepared by dissolving PbI_2 in the co-solvent with varied DMF/DMSO volume ratios (the preferable ratio was 90/10) and then spin-coated on top of the TiO_2 layer at 3000 rpm for 15 s. After drying for 10 min in a glovebox, the substrate was heated at 70 °C for 10 min. The solution of CH_3NH_3I in anhydrous IPA (10 mg mL^{-1}) was spin-coated onto the substrate also at 3000 rpm for 15 s and then annealed at 140 °C for 20 min. For the HTL, the solution of spiro-OMeTAD containing spiro-OMeTAD (80 mg), 4-*tert*-butylpyridine (28.5 μL), and lithium-bis(trifluoromethanesulfonyl)imide (Li-TFSI, 17.5 μL) solution prepared with Li-TFSI (520 mg) in acetonitrile (1 mL), all dissolved in chlorobenzene (1 mL), was spin-coated at 4000 rpm for 30 s. The Au back contact electrode (~80 nm) was prepared via thermal evaporation through a shadow mask under vacuum ($P < 10^{-6}$ Torr) to complete the device fabrication. Each device consisted of four independent pixels with an active area of 0.04 cm^2.

Device Characterization. The devices were characterized in air under AM 1.5G simulated 1 sun irradiation (100 mW cm^{-2}) with a solar simulator (Yamashita Denso) and a source meter (Keithley 2400). The light intensity was calibrated with a silicon photodiode (Hamamatsu S1336-5BK). IPCE spectra were measured with a lock-in amplifier and a current preamplifier under short-circuit conditions and illumination with monochromatic light from a quartz halogen lamp (250 W, Osram) passed through a monochromator (Spectral Products CM110).

Crystal structures were measured by XRD (Bruker D8 DISCOVER, Cu Kα radiation, 40 kV, 40 mA). The surface morphology was characterized with an AFM (Veeco, Innova) and a SEM (JEOL JSM-7401F).

The EIS spectra of all devices were measured under 1 sun illumination with an electrochemical workstation (IM 6, Zahner, Germany) over the frequency range of 100 mHz to 4 MHz; 0.8 V bias voltage and 10 mV AC amplitude were applied during the measurements. The obtained EIS data were fitted (ZView software) based on an equivalent circuit model.

Transient PL decays were recorded with a TCSPC system (FluoTime 200, PicoQuant) using a picosecond pulse diode laser (LDH-635, PicoQuant, full width at half maximum ≈ 70 ps) at 635 nm for excitation; the PL temporal profiles were collected at 770 nm. The pulse energy used for excitation was 15 μJ cm^{-2}.

ASSOCIATED CONTENT

Supporting Information

The Supporting Information is available free of charge on the ACS Publications website at DOI: 10.1021/acsami.7b11795.

SEM images, XRD patterns, SCLC results, hysteresis characteristics, stabilized power output, EIS results, IPCE spectra, and photovoltaic raw data (PDF)

AUTHOR INFORMATION

Corresponding Authors

*E-mail: cshsu@mail.nctu.edu.tw (C.-S.H.).
*E-mail: diau@mail.nctu.edu.tw (E.W.-G.D.).

ORCID

Eric Wei-Guang Diau: 0000-0001-6113-5679

Notes

The authors declare no competing financial interest.

ACKNOWLEDGMENTS

The Taiwan Ministry of Science and Technology (MOST) supported this work with contracts MOST105-2119-M-009-011-MY3, MOST 105-2119-M-009-001, and MOST 104-2221-E-009-179-MY3.

REFERENCES

(1) Kojima, A.; Teshima, K.; Shirai, Y.; Miyasaka, T. Organometal Halide Perovskites as Visible-Light Sensitizers for Photovoltaic Cells. *J. Am. Chem. Soc.* **2009**, *131*, 6050−6051.

(2) Burschka, J.; Dualeh, A.; Kessler, F.; Baranoff, E.; Cevey-Ha, N.-L.; Yi, C.; Nazeeruddin, M. K.; Grätzel, M. Tris(2-(1H-pyrazol-1-yl)pyridine)cobalt(III) as p-type dopant for organic semiconductors and its application in highly efficient solid-state dye-sensitized solar cells. *J. Am. Chem. Soc.* **2011**, *133*, 18042−18045.

(3) Im, J.-H.; Lee, C.-R.; Lee, J.-W.; Park, S.-W.; Park, N.-G. 6.5% efficient perovskite quantum-dot-sensitized solar cell. *Nanoscale* **2011**, *3*, 4088−4093.

(4) Al-Dainy, G. A.; Bourdo, S. E.; Saini, V.; Berry, B. C.; Biris, A. S. Hybrid Perovskite Photovoltaic Devices: Properties, Architecture, and Fabrication Methods. *Energy Technol.* **2017**, *5*, 373−401.

(5) Zhao, Z.; Sun, W.; Li, Y.; Ye, S.; Rao, H.; Gu, F.; Liu, Z.; Bian, Z.; Huang, C. Simplification of device structures for low-cost, high-efficiency perovskite solar cells. *J. Mater. Chem. A* **2017**, *5*, 4756−4773.

(6) Correa-Baena, J.-P.; Abate, A.; Saliba, M.; Tress, W.; Jacobsson, T. J.; Grätzel, M.; Hagfeldt, A. The rapid evolution of highly efficient perovskite solar cells. *Energy Environ. Sci.* **2017**, *10*, 710−727.

(7) Bakr, Z. H.; Wali, Q.; Fakharuddin, A.; Schmidt-Mende, L.; Brown, T. M.; Jose, R. Advances in hole transport materials engineering for stable and efficient perovskite solar cells. *Nano Energy* **2017**, *34*, 271−305.

(8) Yang, G.; Tao, H.; Qin, P.; Ke, W.; Fang, G. Recent progress in electron transport layers for efficient perovskite solar cells. *J. Mater. Chem. A* **2016**, *4*, 3970−3990.

DOI: 10.1021/acsami.7b11795
ACS Appl. Mater. Interfaces 2017, 9, 38530−38536

(9) Wu, W.-Q.; Chen, D.; Caruso, R. A.; Cheng, Y.-B. Recent progress in hybrid perovskite solar cells based on n-type materials. *J. Mater. Chem. A* **2017**, *5*, 10092−10109.
(10) Liu, D.; Kelly, T. L. Perovskite solar cells with a planar heterojunction structure prepared using room-temperature solution processing techniques. *Nat. Photonics* **2013**, *8*, 133−138.
(11) Cai, F.; Yang, L.; Yan, Y.; Zhang, J.; Qin, F.; Liu, D.; Cheng, Y.-B.; Zhou, Y.; Wang, T. Eliminated hysteresis and stabilized power output over 20% in planar heterojunction perovskite solar cells by compositional and surface modifications to the low-temperature-processed TiO_2 layer. *J. Mater. Chem. A* **2017**, *5*, 9402−9411.
(12) Liu, Z.; Chen, Q.; Hong, Z.; Zhou, H.; Xu, X.; De Marco, N.; Sun, P.; Zhao, Z.; Cheng, Y.-B.; Yang, Y. Low-Temperature TiO_x Compact Layer for Planar Heterojunction Perovskite Solar Cells. *ACS Appl. Mater. Interfaces* **2016**, *8*, 11076−11083.
(13) Yin, G.; Ma, J.; Jiang, H.; Li, J.; Yang, D.; Gao, F.; Zeng, J.; Liu, Z.; Liu, S. F. Enhancing Efficiency and Stability of Perovskite Solar Cells through Nb-Doping of TiO_2 at Low Temperature. *ACS Appl. Mater. Interfaces* **2017**, *9*, 10752−10758.
(14) Gubbala, S.; Chakrapani, V.; Kumar, V.; Sunkara, M. K. Band-Edge Engineered Hybrid Structures for Dye-Sensitized Solar Cells Based on SnO_2 Nanowires. *Adv. Funct. Mater.* **2008**, *18*, 2411−2418.
(15) Liu, X.; Yu, H.; Yan, L.; Dong, Q.; Wan, Q.; Zhou, Y.; Song, B.; Li, Y. Triple cathode buffer layers composed of PCBM, C_{60}, and LiF for high-performance planar perovskite solar cells. *ACS Appl. Mater. Interfaces* **2015**, *7*, 6230−6237.
(16) Abrusci, A.; Stranks, S. D.; Docampo, P.; Yip, H.-L.; Jen, A. K.-Y.; Snaith, H. J. High-performance perovskite-polymer hybrid solar cells via electronic coupling with fullerene monolayers. *Nano Lett.* **2013**, *13*, 3124−3128.
(17) Wojciechowski, K.; Stranks, S. D.; Abate, A.; Sadoughi, G.; Sadhanala, A.; Kopidakis, N.; Rumbles, G.; Li, C.-Z.; Friend, R. H.; Jen, A. K.-Y.; Snaith, H. J. Heterojunction Modification for Highly Efficient Organic−Inorganic Perovskite Solar Cells. *ACS Nano* **2014**, *8*, 12701−12709.
(18) Wojciechowski, K.; Ramirez, I.; Gorisse, T.; Dautel, O.; Dasari, R.; Sakai, N.; Hardigree, J. M.; Song, S.; Marder, S.; Riede, M.; Wantz, G.; Snaith, H. J. Cross-Linkable Fullerene Derivatives for Solution-Processed n−i−p Perovskite Solar Cells. *ACS Energy Lett.* **2016**, *1*, 648−653.
(19) Zhang, F.; Song, J.; Chen, M.; Liu, J.; Hao, Y.; Wang, Y.; Qu, J.; Zeng, P. Enhanced perovskite morphology and crystallinity for high performance perovskite solar cells using a porous hole transport layer from polystyrene nanospheres. *Phys. Chem. Chem. Phys.* **2016**, *18*, 32903−32909.
(20) Wu, Y.; Islam, A.; Yang, X.; Qin, C.; Liu, J.; Zhang, K.; Peng, W.; Han, L. Retarding the crystallization of PbI2 for highly reproducible planar-structured perovskite solar cells via sequential deposition. *Energy Environ. Sci.* **2014**, *7*, 2934.
(21) Luo, J.; Peng, L.-M.; Xue, Z. Q.; Wu, J. L. Positive electron affinity of fullerenes: Its effect and origin. *J. Chem. Phys.* **2004**, *120*, 7998−8001.
(22) Tao, C.; Neutzner, S.; Colella, L.; Marras, S.; Kandada, A. R. S.; Gandini, M.; De Bastiani, M.; Pace, G.; Manna, L.; Caironi, M.; Bertarelli, C.; Petrozza, A. 17.6% stabilized efficiency in low-temperature processed planar perovskite solar cells. *Energy Environ. Sci.* **2015**, *8*, 2365−2370.
(23) Xie, X.; Liu, G.; Xu, C.; Li, S.; Liu, Z.; Lee, E.-C. Tuning the work function of indium-tin-oxide electrodes for low-temperature-processed, titanium-oxide-free perovskite solar cells. *Org. Electron.* **2017**, *44*, 120−125.
(24) Chao, Y.-H.; Huang, Y.-Y.; Chang, J.-Y.; Peng, S.-H.; Tu, W.-Y.; Cheng, Y.-J.; Hou, J.; Hsu, C.-S. A crosslinked fullerene matrix doped with an ionic fullerene as a cathodic buffer layer toward high-performance and thermally stable polymer and organic metallohalide perovskite solar cells. *J. Mater. Chem. A* **2015**, *3*, 20382−20388.
(25) Cheng, Y.-J.; Cao, F.-Y.; Lin, W.-C.; Chen, C.-H.; Hsieh, C.-H. Self-Assembled and Cross-Linked Fullerene Interlayer on Titanium Oxide for Highly Efficient Inverted Polymer Solar Cells. *Chem. Mater.* **2011**, *23*, 1512−1518.
(26) Liu, F.; Dong, Q.; Wong, M. K.; Djurišić, A. B.; Ng, A.; Ren, Z.; Shen, Q.; Surya, C.; Chan, W. K.; Wang, J.; Ng, A. M. C.; Liao, C.; Li, H.; Shih, K.; Wei, C.; Su, H.; Dai, J. Is Excess PbI_2 Beneficial for Perovskite Solar Cell Performance? *Adv. Energy Mater.* **2016**, *6*, 1502206.
(27) Zhang, D.; Choy, W. C. H.; Xie, F.; Sha, W. E. I.; Li, X.; Ding, B.; Zhang, K.; Huang, F.; Cao, Y. Plasmonic Electrically Functionalized TiO_2 for High-Performance Organic Solar Cells. *Adv. Funct. Mater.* **2013**, *23*, 4255−4261.
(28) Tsai, C.-M.; Wu, G.-W.; Narra, S.; Chang, H.-M.; Mohanta, N.; Wu, H.-P.; Wang, C.-L.; Diau, E. W.-G. Control of preferred orientation with slow crystallization for carbon-based mesoscopic perovskite solar cells attaining efficiency 15%. *J. Mater. Chem. A* **2017**, *5*, 739−747.
(29) Shiu, J.-W.; Lan, C.-M.; Chang, Y.-C.; Wu, H.-P.; Huang, W.-K.; Diau, E. W.-G. Size Controlled Anatase Titania Single Crystals with Octahedron-like Morphology for Dye-Sensitized Solar Cells. *ACS Nano* **2012**, *6*, 10862−10873.
(30) Ahn, N.; Son, D.-Y.; Jang, I.-H.; Kang, S. M.; Choi, M.; Park, N.-G. Highly Reproducible Perovskite Solar Cells with Average Efficiency of 18.3% and Best Efficiency of 19.7% Fabricated via Lewis Base Adduct of Lead(II) Iodide. *J. Am. Chem. Soc.* **2015**, *137*, 8696−8699.
(31) Hsieh, C.-H.; Cheng, Y.-J.; Li, P.-J.; Chen, C.-H.; Dubosc, M.; Liang, R.-M.; Hsu, C.-S. Highly Efficient and Stable Inverted Polymer Solar Cells Integrated with a Cross-Linked Fullerene Material as an Interlayer. *J. Am. Chem. Soc.* **2010**, *132*, 4887−4893.

DOI: 10.1021/acsami.7b11795
ACS Appl. Mater. Interfaces 2017, 9, 38530−38536